AIMS Mathematics, 8(5): 11202–11220.
DOI: 10.3934/math.2023567
Received: 07 December 2022
Revised: 13 February 2023
Accepted: 22 February 2023
Published: 09 March 2023

http://www.aimspress.com/journal/Math

Research article

Numerical analysis of Darcy resistant Sutterby nanofluid flow with effect of radiation and chemical reaction over stretching cylinder: induced magnetic field

Nadeem Abbas[1], Wasfi Shatanawi[1,2,3,*], Fady Hasan[1] and Taqi A. M. Shatnawi[3]

[1] Department of Mathematics and Sciences, College of Humanities and Sciences, Prince Sultan University, Riyadh 11586, Saudi Arabia
[2] Department of Medical Research, China Medical University Hospital, China Medical University, Taichung 40402, Taiwan
[3] Department of Mathematics, Faculty of Science, The Hashemite University, P.O. Box 330127, Zarqa 13133, Jordan

* **Correspondence:** Email: wshatanawi@psu.edu.sa; Tel: +962799724027.

Abstract: In this analysis, Sutterby nanofluid flow with an induced magnetic field at a nonlinear stretching cylinder is deliberated. The effects of variable thermal conductivity, Darcy resistance, and viscous dissipation are discussed. Thermal radiation and chemical reaction are considered to analyze the impact on the nonlinear stretching cylinder. The governing model of the flow problem is developed under the boundary layer approximation in terms of partial differential equations. Partial differential equations are transformed into ordinary differential equations by performing the suitable transformations. A numerical structure is applied to explain ordinary differential equations. The impact of each governing physical parameters on the temperature, concentration, skin friction, Sherwood, and Nusselt number is presented in graphs and tabular form. Increment in Prandtl number, which declined the curves of the temperature function. Temperature declined because the Prandtl number declined the thermal thickness as well as reduce the temperature of the fluid. Temperature curves showed improvement as Eckert number values increased because the Eckert number is a ratio of kinetic energy to the specific enthalpy difference between the wall and the fluid. As a result, increasing the Eckert number causes the transformation of kinetic energy into internal energy via work done against viscous fluid stresses.

Keywords: stretching cylinder; induced magnetic field; Sutterby nanofluid; Darcy resistance; thermal radiation; variable thermal conductivity
Mathematics Subject Classification: 76A05, 76W99, 80M25, 93A30

Nomenclature

Unit	Term	Unit	Term
$(r,s)(m)$	Curvilinear coordinates	$k_f(W/m^2)$	Thermal conductivity of fluid
$U_w(m/s)$	Wall Velocity	$\nu(m^2/s)$	Kinematic viscosity
$\alpha(m^2/s)$	Thermal diffusivity	$\rho(kg/m^3)$	Fluid density
$(u,v)(m/s)$	velocity components	$\tau(J/kgK)$	Heat capacitance and base fluid ratio
$l(m)$	Length of stretching sheet	$D_B(m^2/s)$	Brownian diffusivity
$T_w(K)$	Wall temperature	$C_p(J/kgK)$	Specific heat capacitance
$C_w(mol/m^3)$	Wall concentration	$T(K)$	Prescribed temperature
Pr (1)	Prandtl number	$Sh_s(1)$	Sherwood number
$Sc(1)$	Schmidt number	τ_{rx}(Pa)	Wall shear stress
$N_B(1)$	Brownian parameter	$N_T(1)$	Thermophoresis parameter
‘	Derivatives with respect to η	$Re_s(1)$	Local Reynold number
γ_0	Curvature parameter	$T_\infty(K)$	Ambient temperature
Ha	Hartmann number	β_1	Sutterby fluid parameter
$\lambda_1(1)$	Sponginess parameter	$\beta_2(1)$	Darcy resistant parameter
$\beta(1)$	Magnetic field parameter	$\epsilon(1)$	Variable thermal conductivity
$Rd(1)$	Thermal radiation	$Q_0(1)$	Heat generation
$Ec(1)$	Eckert number	$Sc(1)$	Schmidt number
$\delta_1(1)$	Chemical reaction	$\lambda(1)$	Magnetic Prandtl number

1. Introduction

One of the most significant issues in real-world problems is the study of non-Newtonian fluids. Because of the collaborative environment, this study is always preferable to viscous fluid in various industrial, physiological, and engineering progressions. The non-Newtonian liquids have not been defined as a single relation for good justifications fact. As a result, the literature suggests using different constitutive connections to include the rheological features. Sutterby fluid is one type of non-Newtonian liquid which a good representation of an aqueous polymer solution. This model is presented as the first by Sutterby [1]. The viscosity data for each solution incorporated a generalized model of Newtonian viscosity that perfectly represented no-shear viscosity. Non-Newtonian Sutterby liquid has been considered with natural convective and uniform heat flux by Tetsu et al. [2]. Shima et al. [3] provided a comprehensive review of Sutterby liquid for bubbles behaviour. Batra and Eissa [4] deliberated the model of Sutterby liquid using the influence of forced convection in the eccentric annulus. Mir et al. [5] discussed the Cattaneo-Christov for Sutterby liquid model using the influence of thermal stratification. The analytical (Homotopy approaches) technique was used to determine the consequences. Sutterby liquid model with Maxwell fluid having the impact of activation energy by Sajid et al. [6]. Numerical results have been developed to achieve the effects on inclined stretching surface. Waqas et al. [7] planned to solve the model of Sutterby fluid having solid nanomaterial

particles under the activation energy across a wedge. The magnetic hydrodynamic bio-convection influence numerical has settled. Rao et al. [8] debated the Sutterby fluid with viscous dissipation over a permeable stretching surface. To solve the problem and highlight the effects under the flow region, the SRS (Spectral Relaxation Scheme) is used. Akram et al. [9] used the Sutterby fluid to analyze the impact of graphene oxide with base fluid as blood under electromagnetic fields. Awan et al. [10] debated the influence of Sutterby liquid on stretching sheets. Salahuddin et al. [11] highlighted the influence of non-Newtonian fluid flow using the surface of catalytic parabolic. Bouslimi et al. [12] discussed the impact of the thermal properties of the Sutterby liquid model. Recently, several authors have studied the Sutterby fluid model to analyze the impact of different rules see [13–16].

In the science field, electrically conducting fluid is a critical contribution to the existence of the magnetic field. The implementation of magnetic hydrodynamics has involved playing an important role in different real fields like geology, mechanical engineering, MHD generators, metallic sensors, astrophysics, cosmology, seismology, the drug industry, and so on. Pavlov [17] pioneered the discussion of the magnetic hydrodynamic impact on viscous fluid. This was one of the most significant initiatives in his analysis. This step developed the essential contribution to real-life problems. Andersson [18] used a viscoelastic fluid model to demonstrate the effect of magnetic hydrodynamics when stretching a sheet. The exact solution has been developed to present the effect of a stretching sheet. Takhar et al. [19] debated magnetic hydrodynamics using chemically reactive fluid at a stretching surface. One of the most attributes of magnetic hydrodynamic flow contributed to the several applications of real life. The induced magnetic field proved the idea by Gailitis et al. [20]. They elaborated on the induced magnetic field using the family of Riga dynamics. Ali et al. [21] considered the stagnation area to find the results of magnetic hydrodynamic flow at the stretching sheet numerically. Sandeep et al. [22] studied the chemically reactive Jeffery fluid under the induced magnetic field effect at the stretching sheet. Al-Hanaya et al. [23] debated the curved surface to analyze the influence of magnetic hydrodynamic hybrid nanomaterial micropolar fluid. Khan et al. [24] deliberated the Burgers nanomaterial liquid model chemically at an exponentially stretching sheet. Amjad et al. [25] used the induced magnetic field for micropolar Casson nanomaterial fluid with stagnation region at a permeable curved surface. Anwar et al. [26] highlighted the influence of Casson hybrid nanomaterial fluid with an induced magnetic field at vertical permeable exponentially sheet. In the decay literature, a few authors developed ideas about the induced magnetic fields for various fluid models see [27–31].

Energy consumption in real life plays one of the most essential roles in every field. Natural energy consumption has been reduced due to the increased use of energy in various fields over time. Due to energy consumption, several methods have been settled to investigate which method of energy enhancement is better. Nanomaterial is one of the best ways to enhance energy in various sectors as compared to conventional fluid. The nanomaterial particles are mixed with the base liquid to improve the thermal conductivity of the base liquid as well as heat transfer phenomena enhancement. There are several sectors where nanofluid is used, namely: electronic sectors, microchips, space airplanes, treatment and diagnosis of various diseases, Pharmaceutical procedures, biomedical devices, vehicle cooling, diagnoses and treatment of different diseases, etc.

Due to various applications, Shukla et al. [32] deliberated the chemically reactive nanofluid having viscous dissipation and MHD impacts. Buongiorno [33] provided the idea of the constitution for equation convective nanofluid. Zaimi et al. [34] deliberated Buongiorno's model using the time-dependent flow in a contracting cylinder. Hassain et al. [35] explored Buongiorno's model for Sisko fluid in the presence of the impact of joule heating and MHD at the stretching cylinder. Ali et al. [36] debated the influence of multi-slip on the time-dependent properties of nanofluid at the stretchable

sheet. Abbas et al. [37] applied the MHD effect on a hybrid nanofluid at the stretching cylinder. Shafey et al. [38] highlighted the consequence of Buongiorno's model for a viscous fluid. Currently, some researchers are studying Buongiorno's model using several rules see [39–44].

The heat and mass transfer of induced magnetic field on Sutterby nanofluid flow over a nonlinear stretching cylinder is considered. The impacts of variable thermal conductivity and viscous dissipation in the presence of chemical reaction are engaged into account. The governing model of the flow problem is developed under the boundary layer approximation in terms of partial differential equations. The partial differential equation transformed into ordinary differential equations using suitable transformations. The ordinary differential equations are elucidated through a numerical structure. The effects governing physical parameters are offered through graphs as well as in tabular form. These results are unique and no one discuss them before.

2. Mathematical formulation

The Sutterby nanofluid flow in the presence of an induced magnetic field at a stretching cylinder has been presented. The x-axis presented the axis of the cylinder and the r-axis presented the radial which reveals in Figure 1.

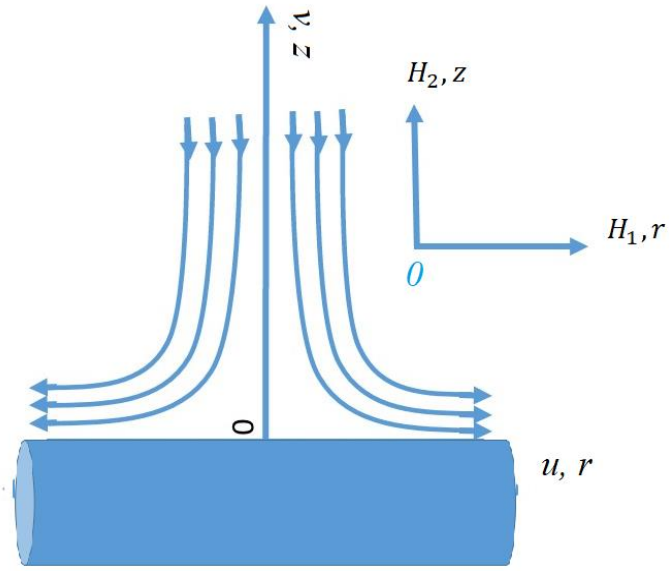

Figure 1. Flow pattern of Sutterby nanofluid over stretching cylinder.

The uniform strength of the magnetic field is H_0 acting along the radial direction. The parallel component of the induced magnetic field H_1 and induced magnetic field applied along the radial direction is assumed as $H_0 = H_e$ in the free stream flow. The normal component H_2 vanished near the wall. T and T_w are fluid temperature and wall temperature respectively. T_∞ is away from the wall temperature which is called ambient temperature. The variable thermal conductivity with heat generation and viscous dissipation having a chemical reaction. The variable thermal conductivity and viscous dissipation are applied on the fluid flow. The velocity component u along the r-axis and velocity component v along the z-axis. a^2 is the consistency index, m is the flow component index, c_p is heat capacity, ρ is the density of fluid, υ_0 kinematic viscosity, magnetic permeability is μ_e, η_0 is magnetic diffusivity. The continuity equation, induced magnetic field equation, momentum

equation and energy equation are presented below under the above flow assumption:

$$\frac{\partial u}{\partial r}+\frac{u}{r}+\frac{\partial v}{\partial z}=0, \tag{1}$$

$$\frac{\partial H_1}{\partial r}+\frac{H_1}{r}+\frac{\partial H_2}{\partial z}=0, \tag{2}$$

$$u\frac{\partial u}{\partial x}+v\frac{\partial v}{\partial r}-\frac{\mu_e}{4\pi\rho_f}\left(H_1\frac{\partial H_1}{\partial x}+H_2\frac{\partial H_1}{\partial r}\right)=\left(\frac{\upsilon_0}{2}\right)\frac{\partial^2 \mathrm{u}}{\partial r^2}+\left(\frac{\upsilon_0}{2}\right)\frac{1}{r}\frac{\partial \mathrm{u}}{\partial r}-\left(\frac{\upsilon_0 m a^2}{4}\right)\left(\frac{\partial \mathrm{u}}{\partial r}\right)^2\frac{\partial^2 \mathrm{u}}{\partial r^2}+\frac{R_z}{\rho_f}-\frac{\sigma B^2}{\rho_f}u, \tag{3}$$

$$u\frac{\partial H_1}{\partial x}+v\frac{\partial H_1}{\partial r}-H_1\frac{\partial u}{\partial x}-H_2\frac{\partial u}{\partial r}=\eta_0\left(\frac{\partial^2 H_1}{\partial r^2}+\frac{1}{r}\frac{\partial H_1}{\partial r}\right), \tag{4}$$

$$u\frac{\partial \mathrm{T}}{\partial x}+v\frac{\partial \mathrm{T}}{\partial r}=\frac{1}{\rho c_p}\frac{1}{r}\frac{\partial}{\partial r}\left(\mathrm{K(T)r}\frac{\partial \mathrm{T}}{\partial r}\right)+Q_1(T-T_\infty)-\frac{\partial q_r}{\partial r}+\frac{\mu}{\rho c_p}\left(\frac{\partial \mathrm{u}}{\partial r}\right)^2+\frac{\tau}{\rho c_p}\left(D_B\frac{\partial \mathrm{C}}{\partial r}\frac{\partial \mathrm{T}}{\partial r}+\frac{D_T}{D_\infty}\left(\frac{\partial \mathrm{T}}{\partial r}\right)^2\right), \tag{5}$$

$$u\frac{\partial \mathrm{C}}{\partial x}+v\frac{\partial \mathrm{C}}{\partial r}=D_B\frac{1}{r}\frac{\partial}{\partial r}\left(\mathrm{r}\frac{\partial \mathrm{C}}{\partial r}\right)+R_1(C-C_\infty)^n+\frac{D_T}{D_\infty}\frac{1}{r}\frac{\partial}{\partial r}\left(\mathrm{r}\frac{\partial \mathrm{T}}{\partial r}\right). \tag{6}$$

With relevant boundary conditions are as following:

$$\begin{aligned} &u=U_w,\ v=0,\ H_1=0,\ H_2=0, T_w=T,\ \text{as}\ r\to a,\\ &u\to 0,\ H_1\to H_e,\ T\to T_\infty,\ \text{as}\ r\to\infty. \end{aligned} \tag{7}$$

Introducing the stream functions are:

$$u=\frac{1}{r}\frac{\partial\psi}{\partial r}, v=-\frac{1}{r}\frac{\partial\psi}{\partial x}, H_1=\frac{1}{r}\frac{\partial\psi_1}{\partial r}, H_2=-\frac{1}{r}\frac{\partial\psi_1}{\partial x}, \eta=\frac{r^2-a^2}{2a}\sqrt{\frac{U_w}{\upsilon_f x}},$$

$$T=T_\infty+(T_w-T_\infty)\theta(\eta), C=C_\infty+(C_w-\mathrm{C})\phi(\eta). \tag{8}$$

$\psi_1=H_o a\sqrt{\frac{\upsilon_f}{U_w}}\mathrm{G}(\eta)$ and $\psi=\sqrt{2U_w\upsilon_f x}aF(\eta)$ are the stream functions of magnetic field and velocity. Using the above suitable transformation and the partial differential equations become ordinary differential equations as below:

$$\begin{aligned} &(1+2\eta\gamma_0)f'''(\eta)+2f''(\eta)f(\eta)-\left(f'(\eta)\right)^2-\frac{\beta_1}{2}(1+2\eta\gamma_0)^2(f''(\eta))^2f'''(\eta)\\ &-\left(Ha+\frac{\lambda_1}{2}\right)f'(\eta)+\frac{1}{12}\beta_2\left(f''(\eta)\right)^2f'(\eta)+\beta(G'(\eta)G'(\eta)-G(\eta)G''(\eta))=0, \end{aligned} \tag{9}$$

$$\lambda(1+2\eta\gamma_0)G'''(\eta)+2\lambda\gamma G''(\eta)+G(\eta)F''(\eta)-G''(\eta)F(\eta)=0, \tag{10}$$

$$\begin{aligned} &\frac{1}{Pr}\left(1+\epsilon\theta(\eta)+\frac{4}{3}Rd\right)(1+2\eta\gamma_0)\theta''+\left(PrF(\eta)+\gamma_0+\epsilon\gamma_0\theta(\eta)+\frac{4}{3}Rd\gamma_0\right)\theta'(\eta)\\ &+PrQ_0\theta(\eta)+PrEc(F''(\eta))^2+N_T\theta'(\eta)\theta'(\eta)+N_B\theta'(\eta)\phi'(\eta)=0, \end{aligned} \tag{11}$$

$$(1+2\eta\gamma_0)\phi''(\eta)+\frac{N_T}{N_B}\theta''(\eta)+2\gamma_0\left(\theta'(\eta)+\phi'(\eta)\right)-Sc\phi'(\eta)f(\eta)-Sc\delta_1\left(\phi(\eta)\right)^n. \tag{12}$$

With boundary condition

$$F(0)=0, F'(0)=1, F'(\infty)=0, G(0)=0, G'(0)=0,$$
$$G'(\infty)=1, \theta(0)=1, \theta(\infty)=0, \phi(0)=1, \phi(\infty)=0. \quad (13)$$

Where, γ_0 (Curvature parameter), Ha (Hartmann number), β_1 (Sutterby fluid parameter), λ_1(Sponginess parameter), β_2(Darcy resistant parameter), β(Magnetic field parameter), ϵ(Variable thermal conductivity), Rd (Thermal radiation), Q_0 (Heat generation), Ec (Eckert number), N_T(Thermophoresis), N_B(Brownian), Sc(Schmidt number), δ_1(Chemical reaction) and λ(Magnetic Prandtl number). The presentation of these quantities is defined as:

$$C_f=\frac{2[\tau_w]_{r=a}}{\rho(U_w)^2}, N_u=\frac{x\left(1+\frac{4}{3}Rd\right)\left[\frac{\partial T}{\partial r}\right]_{r=a}}{k\left((T_w-T_\infty)\right)}, S_h=\frac{x\left[\frac{\partial C}{\partial r}\right]_{r=a}}{D_B(C_w-C_\infty)},$$
$$\tau_w=\left(\frac{\partial u}{\partial x}+\frac{\partial v}{\partial r}\right)-\frac{\mu\omega b^2}{12}\left(\frac{\partial u}{\partial x}+\frac{\partial v}{\partial r}\right)\left(2\left(\left(\frac{\partial u}{\partial x}\right)^2+\left(\frac{\partial v}{\partial r}\right)^2+\left(\frac{u}{r}\right)^2\right)+\left(\frac{\partial u}{\partial x}+\frac{\partial v}{\partial r}\right)^2\right). \quad (14)$$

The dimensionless form is presented as

$$C_f{}^S=\left(\frac{\partial^2 f}{\partial\eta^2}-\frac{1}{6}\left[(1+2\eta\gamma_0)\left(\frac{\partial^2 f}{\partial\eta^2}\right)^2+3\left(\frac{\partial f}{\partial\eta}\right)^2-2(1+2\eta\gamma_0)f\frac{\partial f}{\partial\eta}+3(1+2\eta\gamma_1)(f^2)\right]\right)_{\eta\to 0},$$
$$S^n{}_h=-\frac{\partial\Phi}{\partial\eta}_{\eta\to 0}, N^n{}_u=-\left(1+\tfrac{4}{3}Rd\right)\frac{\partial\theta}{\partial\eta}_{\eta\to 0}. \quad (15)$$

3. Numerical procedure

A numerical method called bvp4c is used to explain the dimensionless system (ODE's). The nonlinear boundary value problem that arises in fluid dynamics has been clarified using a variety of techniques. The higher-order nonlinear differential equations yield first-order differential equations. The procedure is defined as follows (see [45]):

$$S(1)=f(\eta), S(2)=f'^{(\eta)}, S(3)=f''^{(\eta)}, SS1=f'''^{(\eta)}, \quad (16)$$

$$SS1=\left(\frac{-1}{1+2x\gamma_0-\frac{\beta_1}{2}(1+2x\gamma_0)^2S(3)S(3)}\right)(2S(3)S(1)-S(2)S(2)$$
$$-\tfrac{\beta_1}{2}(1+2x\gamma_0)^2\left(\tfrac{1}{12}\beta_2S(3)S(3)S(2)\right)+\beta\big(S(5)S(5)-S(6)S(4)\big)-\left(Ha+\tfrac{\lambda_1}{2}\right)S(2)), \quad (17)$$

$$S(4)=G(\xi), S(5)=G'^{(\xi)}, S(6)=G''^{(\xi)}, SS2=G'''^{(\xi)}, \quad (18)$$

$$SS2=\left(\tfrac{-1}{\lambda(1+2x\gamma_0)}\right)(2\lambda\gamma_0S(6)+S(5)S(3)-S(6)S(1)), \quad (19)$$

$$S(7)=\theta(\eta), S(8)=\theta'^{(\eta)}, SS3=\theta''^{(\eta)}, \quad (20)$$

$$SS3 = \left(\frac{-1}{\left(1+\epsilon S(7)+\frac{4}{3}Rd\right)(1+2x\gamma_0)}\right)((\gamma_0+\epsilon\gamma_0 s(7)+\frac{4}{3}Rd\gamma_0)S(8)+PrQ_0S(7)$$

$$+PrS(1)S(8)+PrEc(S(3))^2+PrN_TS(8)S(8)+PrN_BS(8)S(10) \quad (21)$$

$$S(9)=\phi(\eta), S(10)=\phi'^{(\eta)}, SS4=\phi''^{(\eta)}, \quad (22)$$

$$SS4=\left(\frac{-1}{(1+2x\gamma_0)}\right)\left(\frac{N_T}{N_B}SS3+2\gamma_0S(8)+2\gamma_0S(10)-ScS(10)S(1)-Sc\delta_1(S(9))^n\right); \quad (23)$$

With boundary condition

$$S0(1), S0(2)=1, Sinf(2), 0(4), S0(5),$$

$$Sinf(5)=1, S0(7)-1, Sinf(7), S0(9)-1, Sinf(9). \quad (24)$$

4. Results and discussion

The dimensionless form of differential equations is solved through numerical techniques. Graphs and a numerical table are used to present the results of involving physical parameters. Figures 2–9 reveal the variation of the temperature function involving parameters such as Brownian motion, Chemical reaction, Chemical reaction, Schmidt number, Prandtl number, Heat generation, Radiation, and Heat generation. The Significance of Brownian motion on temperature function is publicised in Figure 2. Curves of temperature revealed improvement as the values of the Brownian motion parameter improved. Due to this phenomenon, the various values of nanoparticles have varying quantities of the Brownian parameter because the quantity of nanoparticles increased due to increasing values of the Brownian motion parameter, which improved the heat transfer of the fluid at the surface. The import of variable thermal conductivity on the temperature function is publicised in Figure 3.

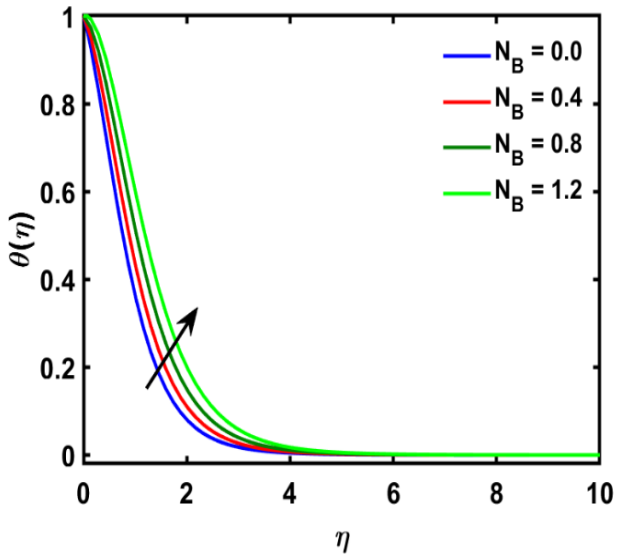

Figure 2. Variation of $\theta(\eta)$ and N_B.

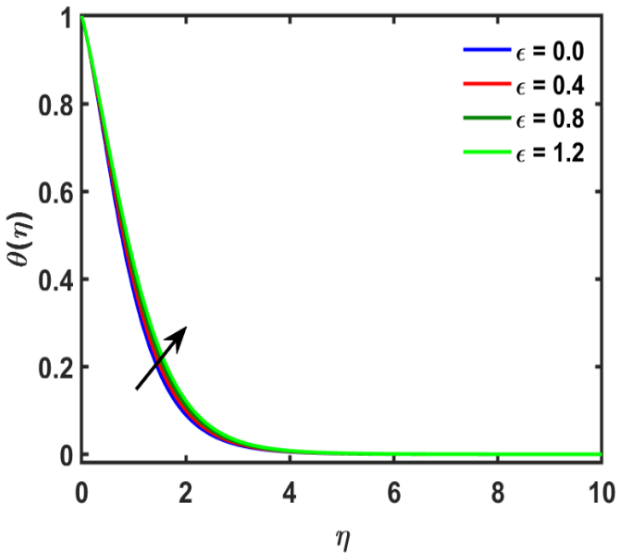

Figure 3. Variation of $\theta(\eta)$ and ϵ.

Influence of thermophoresis on temperature function is publicised in Figure 4. Curves of temperature revealed improvement as the values of the thermophoresis parameter improved. The transport force that occurs due to the existence of a temperature gradient is known as thermophoresis. So the thermophoresis values revealed boosting, which improved the temperature at surface of a cylinder. Figure 5 illustrates the impact of the Eckert number on temperature function. Curves of temperature revealed improvement as the values of Eckert number improved. Because Eckert number is a ratio of kinetic energy to the specific enthalpy difference between the wall and the fluid. As a result, increasing the Eckert number causes the transformation of kinetic energy into internal energy via work done against viscous fluid stresses. Figure 6 depicts the variation of the temperature function and the Prandtl number. Increment in the Prandtl number which declined the curves of temperature function. Temperature declined because Prandtl number decreased the thermal thickness as well as the temperature of the fluid.

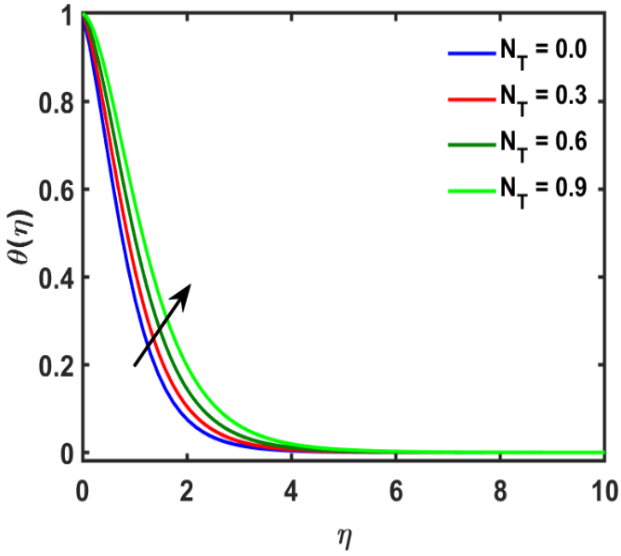

Figure 4. Variation of $\theta(\eta)$ and N_T.

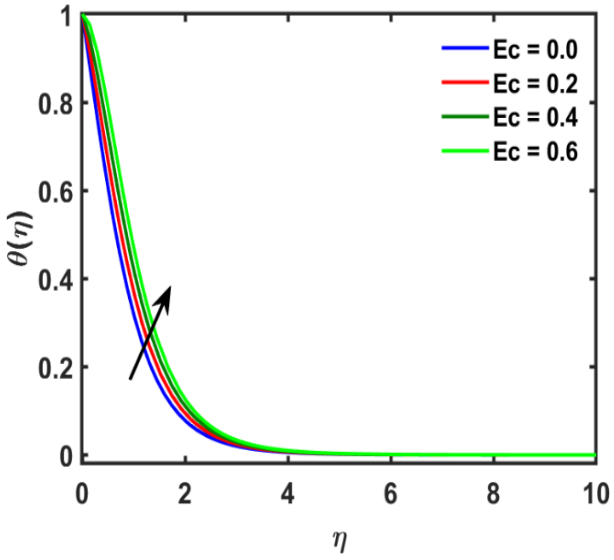

Figure 5. Variation of $\theta(\eta)$ and Ec.

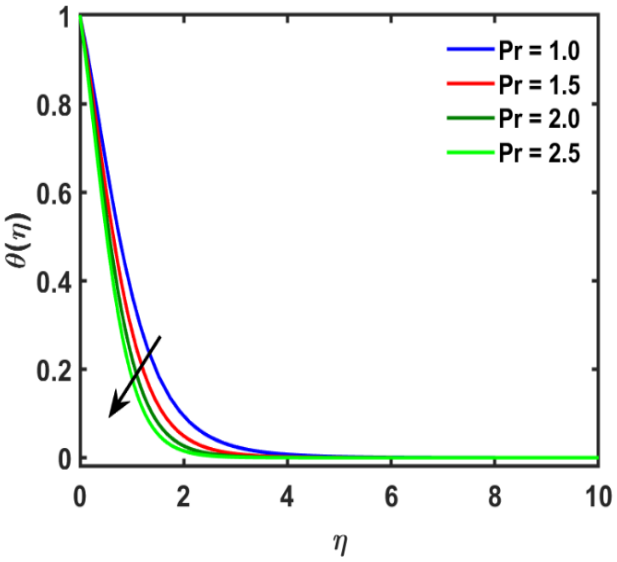

Figure 6. Variation of $\theta(\eta)$ and Pr.

The variation in temperature function and heat generation have been publicised in Figure 7. Increment in heat generation, which boosted the curves of temperature function. Due to higher values of heat generation which improved the temperature at the surface of a cylinder. Higher physically produces more heat in the fluid system, enhancing the temperature profile. As a result, when the heat generation parameter succeeds, a significant amount of heat will be produced, potentially raising the fluid's temperature profile.

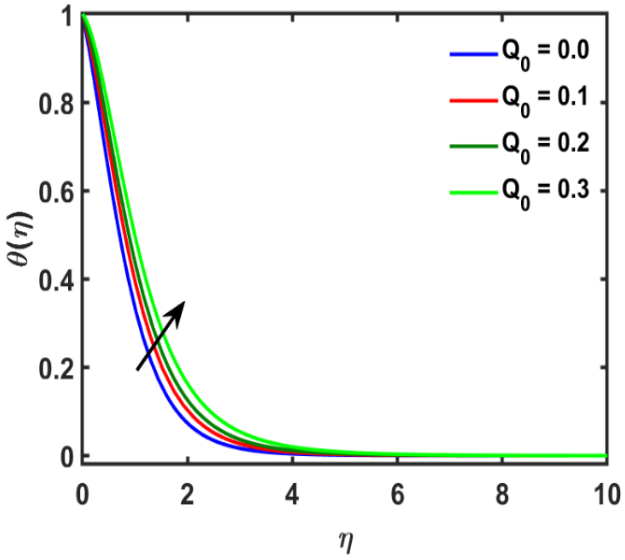

Figure 7. Variation of $\theta(\eta)$ and Q_0.

Figure 8 revealed the impact of radiation on temperature function. The temperature function improved due to boosting values of radiation. This occurs because the Rosseland radiative absorptivity is decreasing, which causes the divergence of the radiative heat change to grow. This causes the rate of radiative heat transmission to the fluid to increase, raising the fluid temperature in the process.

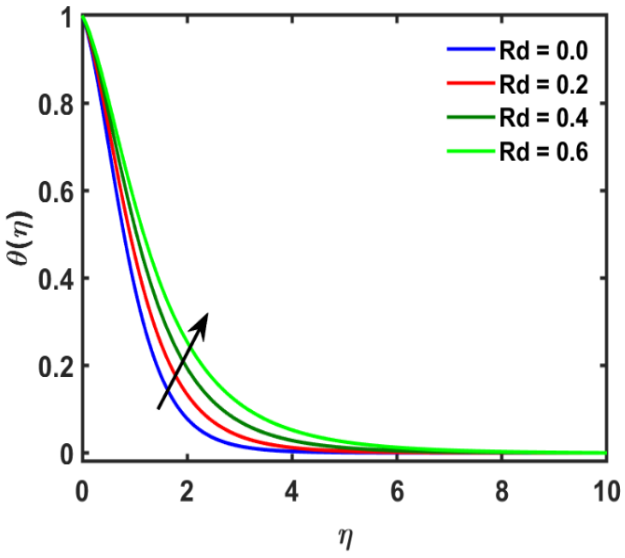

Figure 8. Variation of $\theta(\eta)$ and Rd.

Figures 9–11 publicized the influence of involving parameters such as chemical reaction, Schmidt number, and thermophoresis on the Schmidt number on concentration function. Figure 9 debated the influence of chemical reaction on the concentration. The concentration curves declined due to higher values of chemical reactions. Figure 10 revealed the impact of the Schmidt number on the concentration function. Concentration function values dropped due to boosting values of Schmidt number. Figure 11 revealed the impact of thermophoresis on concentration function. Concentration function values dropped due to boosting values of thermophoresis.

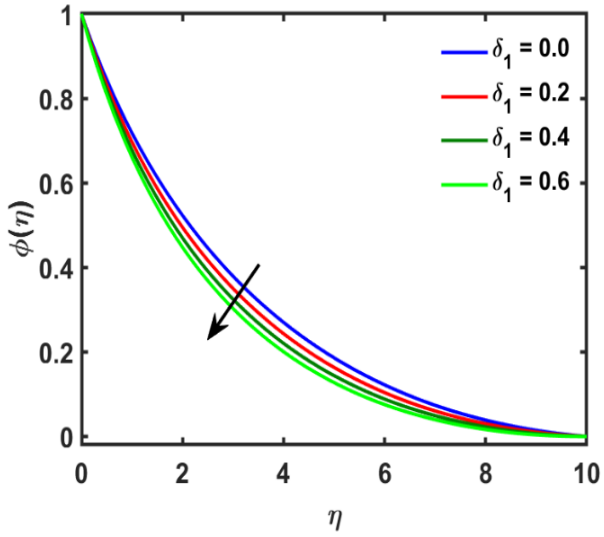

Figure 9. Variation of $\phi(\eta)$ and δ_1.

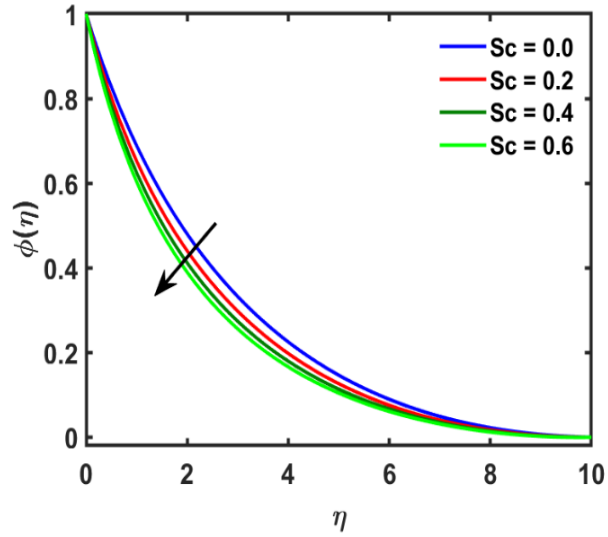

Figure 10. Variation of $\phi(\eta)$ and Sc.

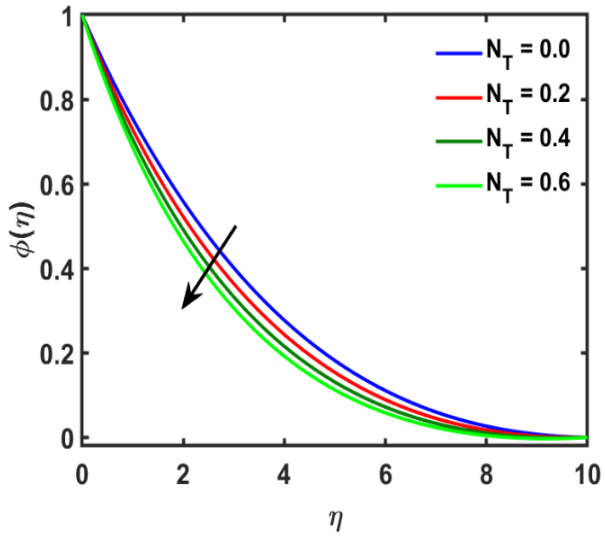

Figure 11. Variation of $\phi(\eta)$ and N_T.

Table 1 publicized the variation of physical parameters namely: Curvature parameter, Hartmann number, Sutterby fluid parameter, Sponginess parameter, Darcy resistant parameter, magnetic field parameter, variable thermal conductivity, Thermal radiation, heat generation, Eckert number, thermophoresis, Brownian, Schmidt number, chemical reaction and magnetic Prandtl number on the skin friction, Nusselt number and Sherwood number. The values of $f''(0)$ have seen no change by implementing the various values of the Eckert number. The quantity of $-\phi'(0)$ and Eckert number have the same behaviour of growing but $-\theta'(0)$ and Eckert number have found to be opposite behaviour.

The link between the kinetic energy in the flow and the enthalpy is expressed by the Eckert number because the Sherwood number improved while the Nusselt number deteriorated due to higher values of the Eckert number. The quantity of $f''(0)$ and $-\theta'(0)$ revealed declining but $-\phi'(0)$ revealed increased due to boosting values of curvature parameter. The surface area increased due to an increment in curvature parameter which the surface become smooth as well as friction reduced. As the curvature increased which increasing the surface ultimately, heat transfer reduced. The quantity of $f''(0)$ and $-\phi'(0)$ revealed boosting but $-\theta'(0)$ revealed diminished due to boosting values of Hartmann number.

The values of $f''(0)$ have seen no change when different values of the Brownian factor have changed. The quantity of $-\phi'(0)$ and Brownian factor have the same behaviour of growing but $-\theta'(0)$ and Brownian factor have been found to be opposite behaviour. The quantity of $f''(0)$ and $-\phi'(0)$ revealed boosting but $-\theta'(0)$ revealed diminishing due to boosting values of the Sutterby fluid parameter. When different values of the Schmidt number have changed, the values of $f''(0)$ have not changed. The quantity of $-\phi'(0)$ and $-\theta'(0)$ declined due to boosting values of Schmidt number. The quantity of $-\phi'(0)$ and $-\theta'(0)$ boosted due to boosting values of a chemical reaction. The quantity of $f''(0)$ and $-\phi'(0)$ revealed boosting but $-\theta'(0)$ revealed diminishing due to boosting values of Sponginess parameter. The quantity of $f''(0)$ and $-\phi'(0)$ revealed diminishing but $-\theta'(0)$ revealed enlarging due to boosting values of Darcy resistant parameter. The values of $f''(0)$ are diminishing when the quantity of Magnetic field parameters improved. The quantity of $-\theta'(0)$ and magnetic field parameter have the same behaviour of growing, but $-\phi'(0)$ and magnetic field parameter have the opposite behaviour.

The values of $f''(0)$ are constant when the quantity of variable thermal conductivity improved. The quantity of $-\theta'(0)$ and variable thermal conductivity have same behaviour of growing but $-\phi'(0)$ and variable thermal conductivity have found to be the opposite behaviour. The values of $f''(0)$ have seen no changing when the quantity of thermal radiation improved. The quantity of $-\theta'(0)$ and thermal radiation have same behaviour of growing but $-\phi'(0)$ and Thermal radiation have found to be opposite behaviour.

It is seen that there is no effect on the $f''(0)$ when different values of heat generation have changed. The quantity of $-\phi'(0)$ and Heat generation have the same behaviour of growing but $-\theta'(0)$ and Heat generation are opposite behaviour. The values of $f''(0)$ have seen no changing when different values of thermophoresis have changed. The quantity of $-\phi'(0)$ and $-\theta'(0)$ declined due to boosting values of thermophoresis. The values remain constant of $f''(0)$ for various values of a chemical reaction. The quantity of $f''(0)$ and $-\phi'(0)$ revealed boosting but $-\theta'(0)$ revealed diminished due to boosting values of magnetic Prandtl.

Table 1. Significant numerical results of $f''(0)$, $-\theta'(0)$ and $-\phi'(0)$ for various values of physical parameters.

γ_0	Ha	β_1	λ_1	β_2	β	ϵ	Rd	Q_0	Ec	N_T	N_B	Sc	δ_1	λ	$f''(0)$	$\theta'(0)$	$\phi'(0)$
0.1	0.4	0.5	0.3	0.5	0.4	0.2	0.2	0.5	0.5	0.5	0.3	0.2	0.1	0.3	1.3124	0.3571	0.5319
0.3															1.2940	0.1842	1.0039
0.5															1.2719	0.1567	1.2986
0.7															1.2252	0.1481	1.5467
0.3	0.0														1.0640	0.2482	0.9386
	0.2														1.1777	0.2164	0.9711
	0.4														1.2940	0.1842	1.0039
	0.6														1.4154	0.1518	1.0367
	0.4	0.1													1.1884	0.1930	0.9949
		0.3													1.2320	0.1890	0.9989
		0.5													1.2940	0.1842	1.0039
		0.7													1.4095	0.1776	1.0106
		0.5	0.1												1.2354	0.2003	0.9875
			0.2												1.2646	0.1922	0.9957
			0.3												1.2940	0.1842	1.0039
			0.4												1.3237	0.1761	1.0121
			0.3	0.3											1.2992	0.1836	1.0045
				0.5											1.2940	0.1842	1.0039
				0.7											1.2888	0.1848	1.0033
				0.9											1.2837	0.1853	1.0027
				0.5	0.2										1.4280	0.1122	1.0761
					0.4										1.2940	0.1842	1.0039
					0.6										1.1499	0.2558	0.9310
					0.8										1.0045	0.3180	0.8664
					0.4	0.0									1.2940	0.1461	1.0417
						0.1									1.2940	0.1664	1.0215

Continued on next page

γ_0	Ha	β_1	λ_1	β_2	β	ϵ	Rd	Q_0	Ec	N_T	N_B	Sc	δ_1	λ	$f''(0)$	$\theta'(0)$	$\phi'(0)$
						0.2									1.2940	0.1842	1.0039
						0.3									1.2940	0.1998	0.9883
						0.2	0.0								1.2940	0.1319	1.0565
							0.1								1.2940	0.1604	1.0278
							0.2								1.2940	0.1842	1.0039
							0.3								1.2940	0.2043	0.9836
							0.2	0.1							1.2940	0.1854	0.9488
								0.3							1.2940	0.1848	0.9767
								0.5							1.2940	0.1842	1.0039
								0.7							1.2940	0.1836	1.0304
								0.5	0.1						1.2940	0.3246	0.8658
									0.3						1.2940	0.2543	0.9349
									0.5						1.2940	0.1842	1.0039
									0.7						1.2940	0.1141	1.0728
									0.5	0.1					1.2940	0.2544	1.1647
										0.3					1.2940	0.2180	1.0376
										0.5					1.2940	0.1842	1.0039
										0.7					1.2940	0.1528	0.9837
										0.5	0.1				1.2940	0.2372	0.8953
											0.3				1.2940	0.2101	0.9371
											0.5				1.2940	0.1842	1.0039
											0.7				1.2940	0.1592	1.0944
											0.5	0.0			1.2940	0.1838	0.9817
												0.2			1.2940	0.1842	1.0039
												0.4			1.2940	0.1845	1.0270
												0.6			1.2940	0.1848	1.0507
												0.2	0.1		1.2940	0.1842	1.0039
													0.2		1.2940	0.1001	1.0845
													0.3		1.2940	0.0096	1.1712
													0.4		1.2940	0.0025	1.2649
													0..1	0.1	1.1632	0.7036	0.8769
														0.3	1.2940	0.1842	1.0039
														0.5	1.4162	0.1201	1.0683
														0.7	1.4432	0.1054	1.0829

Table 2 compares the competitive results of Qasim et al. [44] and Suleman et al. [45] with our results.

Table 2. Comparative results with decay literature for different values of Pr and rest of values zero.

γ_1	Pr	Qasim et al. [44]	Suleman et al. [45]	Present results
0.0	0.720	1.23664	1.236651	1.23663421
	1.000	1.00000	1.000000	1.0000000
	6.700	0.33330	0.333310	0.33330874
	10.00	0.26876	0.268770	0.26871232
1.00	0.720	0.87018	0.870190	0.87017953
	1.000	0.74406	0.744070	0.74405871
	6.700	0.29661	0.296620	0.29660957
	10.00	0.24217	0.242180	0.24216492

5. Conclusions

Heat and mass transfer of Sutterby fluid with induced MHD are considered at a stretching cylinder. The impacts of temperature-dependent properties and viscous dissipation are discussed. Graphs and tables are used to show the effect of physical parameters. The main results are presented as follows:

- The quantity of $f''(0)$ and $-\theta'(0)$ revealed declining but $-\phi'(0)$ revealed increased due to boosting values of curvature parameter. The surface area increased due to an increment in curvature parameter which surface become smooth as well as friction reduced. Heat transfer decreased as the curvature increased, which increased the surface.
- The curves of temperature revealed improvements as the values of Brownian motion improved. Due to this phenomenon, the various values of nanoparticles have various quantities of the Brownian parameter because the number of nanoparticles increased due to increasing values of the Brownian motion parameter, which improved the heat transfer of the fluid at the surface.
- The values of $f''(0)$ are diminishing when the quantity of the magnetic field improved. The quantities of $-\theta'(0)$ and magnetic field parameter both grow in the same way, but $-\phi'(0)$ and the magnetic field parameter have the opposite behaviour.
- Increment in Prandtl number, which declined the curves of temperature function. The temperature declined because Prandtl number declined the thermal thickness as well as the temperature of the fluid.
- The curves of temperature showed improvements as the Eckert number values improved. Because the Eckert number is a ratio of kinetic energy to specific enthalpy difference between the wall and the fluid. As a result, increasing the Eckert number causes the transformation of kinetic energy into internal energy via work done against viscous fluid stresses.

Acknowledgments

Nadeem Abbas, Wasfi Shatanawi, and Fady Hasan wish to express their gratitude to Prince Sultan University for facilitating the publication of this article through the Theoretical and Applied Sciences Lab (TAS).

Conflict of interest

The authors declare no conflicts of interest.

References

1. J. L. Sutterby, Laminar converging flow of dilute polymer solutions in conical sections. II, *Trans. Soc. Rheol.*, **9** (1965), 227–241. https://doi.org/10.1122/1.549024
2. T. Fujii, O. Miyatake, M. Fujii, H. Tanaka, K. Murakami, Natural convective heat-transfer from a vertical surface of uniform heat flux to a non-newtonian sutterby fluid, *Int. J. Heat Mass Transfer*, **17** (1974), 149–154. https://doi.org/10.1016/0017-9310(74)90048-9
3. A. Shima, T. Tsujino, K. Yokoyama, The behavior of bubbles in Sutterby model fluids, *Rep. Inst. High Speed Mech. Tohoku Univ.*, **49** (1984), 39–52.
4. R. L. Batra, M. Eissa, Laminar forced convection heat transfer of a Sutterby model fluid in an eccentric annulus, *Mech. Res. Commun.*, **21** (1994), 147–152. https://doi.org/10.1016/0093-6413(94)90087-6
5. S. Ur Rehman, N. A. Mir, M. S. Alqarni, M. Farooq, M. Y. Malik, Analysis of heat generation/absorption in thermally stratified Sutterby fluid flow with Cattaneo-Christov theory, *Microsyst. Technol.*, **25** (2019), 3365–3373. https://doi.org/10.1007/s00542-019-04522-z
6. T. Sajid, S. Tanveer, Z. Sabir, J. L. G. Guirao, Impact of activation energy and temperature-dependent heat source/sink on maxwell-Sutterby fluid, *Math. Probl. Eng.*, **2020** (2020), 1–15. https://doi.org/10.1155/2020/5251804
7. H. Waqas, U. Farooq, M. M. Bhatti, S. Hussain, Magnetized bioconvection flow of Sutterby fluid characterized by the suspension of nanoparticles across a wedge with activation energy, *J. Appl. Math. Mech.*, **101** (2021), e202000349. https://doi.org/ 10.1002/zamm.202000349
8. M. V. S. Rao, K. Gangadhar, P. R. S. Babu, Sutterby fluid flow past a stretching sheet embedded in a porous media with viscous dissipation, *Int. J. Ambient Energy*, **43** (2022), 5247–5257. https://doi.org/10.1080/01430750.2021.1945491
9. J. Akram, N. S. Akbar, D. Tripathi, Blood-based graphene oxide nanofluid flow through capillary in the presence of electromagnetic fields: a Sutterby fluid model, *Microvasc. Res.*, **145** (2022), 104435. https://doi.org/10.1016/j.mvr.2022.104435
10. A. U. Awan, S. A. A. Shah, H. Waqas, Thermally radioactive bioconvection of magnetized Sutterby nanofluid over a stretching cylinder, *Res. Square*, 2022. https://doi.org/10.21203/rs.3.rs-1361392/v1
11. T. Salahuddin, Z. Ali, M. Awais, M. Khan, M. Altanji, A flow behavior of Sutterby nanofluid near the catalytic parabolic surface, *Int. Commun. Heat Mass Transfer*, **131** (2022), 105821. https://doi.org/10.1016/j.icheatmasstransfer.2021.105821
12. J. Bouslimi, A. A. Alkathiri, T. M. Althagafi, W. Jamshed, M. R. Eid, Thermal properties, flow and comparison between Cu and Ag nanoparticles suspended in sodium alginate as Sutterby nanofluids in solar collector, *Case Stud. Therm. Eng.*, **39** (2022), 102358. https://doi.org/10.1016/j.csite.2022.102358
13. W. Jamshed, M. R. Eid, R. Safdar, A. A. Pasha, S. S. P. Mohamed Isa, M. Adil, et al., Solar energy optimization in solar-HVAC using Sutterby hybrid nanofluid with Smoluchowski temperature conditions: a solar thermal application, *Sci. Rep.*, **12** (2022), 11484. https://doi.org/10.1038/s41598-022-15685-7

14. T. Sajid, W. Jamshed, F. Shahzad, E. K. Akgül, K. S. Nisar, M. R. Eid, Impact of gold nanoparticles along with Maxwell velocity and Smoluchowski temperature slip boundary conditions on fluid flow: Sutterby model, *Chin. J. Phys.*, **77** (2022), 1387–1404. https://doi.org/10.1016/j.cjph.2021.11.011
15. F. Shahzad, J. Bouslimi, S. Gouadria, W. Jamshed, M. R. Eid, R. Safdar, et al., Hydrogen energy storage optimization in solar-HVAC using Sutterby nanofluid via Koo-Kleinstreuer and Li (KKL) correlations model: a solar thermal application, *Int. J. Hydrogen Energy*, **47** (2022), 18877–18891. https://doi.org/10.1016/j.ijhydene.2022.04.039
16. J. Bouslimi, A. A. Alkathiri, A. N. Alharbi, W. Jamshed, M. R. Eid, M. L. Bouazizi, Dynamics of convective slippery constraints on hybrid radiative Sutterby nanofluid flow by Galerkin finite element simulation, *Nanotechnol. Rev.*, **11** (2022), 1219–1236. https://doi.org/10.1515/ntrev-2022-0070
17. K. B. Pavlov, Magnetohydrodynamic flow of an incompressible viscous fluid caused by deformation of a plane surface, *Magnetohydrodynamics*, **4** (1974), 146–147.
18. H. I. Andersson, MHD flow of a viscoelastic fluid past a stretching surface, *Acta Mech.*, **95** (1992), 227–230. https://doi.org/10.1007/BF01170814
19. H. S. Takhar, A. J. Chamkha, G. Nath, Flow and mass transfer on a stretching sheet with a magnetic field and chemically reactive species, *Int. J. Eng. Sci.*, **38** (2000), 1303–1314. https://doi.org/10.1016/S0020-7225(99)00079-8
20. A. Gailitis, O. Lielausis, S. Dement'ev, E. Platacis, A. Cifersons, G. Gerbeth, et al., Detection of a flow induced magnetic field eigenmode in the Riga dynamo facility, *Phys. Rev. Lett.*, **84** (2000), 4365. https://doi.org/10.1103/PhysRevLett.84.4365
21. F. M. Ali, R. Nazar, N. M. Arifin, I. Pop, MHD stagnation-point flow and heat transfer towards stretching sheet with induced magnetic field, *Appl. Math. Mech.*, **32** (2011), 409–418. https://doi.org/10.1007/s10483-011-1426-6
22. N. Sandeep, C. Sulochana, I. L. Animasaun, Stagnation-point flow of a Jeffrey nanofluid over a stretching surface with induced magnetic field and chemical reaction, *Int. J. Eng. Res. Afr.*, **20** (2016), 93–111. https://doi.org/10.4028/www.scientific.net/JERA.20.93
23. A. M. Al-Hanaya, F. Sajid, N. Abbas, S. Nadeem, Effect of SWCNT and MWCNT on the flow of micropolar hybrid nanofluid over a curved stretching surface with induced magnetic field, *Sci. Rep.*, **10** (2020), 1–18. https://doi.org/10.1038/s41598-020-65278-5
24. M. N. Khan, S. Nadeem, N. Abbas, A. M. Zidan, Heat and mass transfer investigation of a chemically reactive Burgers nanofluid with an induced magnetic field over an exponentially stretching surface, *Proc. Inst. Mech. Eng. Part E*, **235** (2021), 2189–2200. https://doi.org/10.1177/09544089211034941
25. M. Amjad, I. Zehra, S. Nadeem, N. Abbas, A. Saleem, A. Issakhov, Influence of Lorentz force and induced magnetic field effects on Casson micropolar nanofluid flow over a permeable curved stretching/shrinking surface under the stagnation region, *Surf. Int.*, **21** (2020), 100766. https://doi.org/10.1016/j.surfin.2020.100766
26. M. I. Anwar, H. Firdous, A. Al Zubaidi, N. Abbas, S. Nadeem, Computational analysis of induced magnetohydrodynamic non-Newtonian nanofluid flow over nonlinear stretching sheet, *Prog. React. Kinet. Mech.*, **47** (2022). https://doi.org/10.1177/14686783211072712

27. T. A. Shatnawi, N. Abbas, W. Shatanawi, Comparative study of Casson hybrid nanofluid models with induced magnetic radiative flow over a vertical permeable exponentially stretching sheet, *AIMS Math.*, **7** (2022), 20545–20564. https://doi.org/10.3934/math.20221126
28. N. Abbas, S. Nadeem, M. N. Khan, Numerical analysis of unsteady magnetized micropolar fluid flow over a curved surface, *J. Therm. Anal. Calorim.*, **147** (2022), 6449–6459. https://doi.org/10.1007/s10973-021-10913-0
29. Y. Nawaz, M. S. Arif, K. Abodayeh, M. Bibi, Finite element method for non-Newtonian radiative Maxwell nanofluid flow under the influence of heat and mass transfer, *Energies*, **15**(2022), 4713. https://doi.org/10.3390/en15134713
30. Y. Nawaz, M. S. Arif, K. Abodayeh, A third-order two-stage numerical scheme for fractional Stokes problems: A comparative computational study, *J. Comput. Nonlinear Dyna.*, **17** (2022), 101004. https://doi.org/10.1115/1.4054800
31. Y. Nawaz, M. S. Arif, K. Abodayeh, Predictor-corrector scheme for electrical magnetohydrodynamic (MHD) Casson nanofluid flow: a computational study, *Appl. Sci.*, **13** (2023), 1209. https://doi.org/10.3390/app13021209
32. N. Shukla, P. Rana, O. A. Beg, B. Singha, Effect of chemical reaction and viscous dissipation on MHD nanofluid, *AIP Conf. Proc.*, **1802** (2017), 020015. https://doi.org/10.1063/1.4973265
33. J. Buongiorno, Convective transport in nanofluids, *J. Heat Transfer*, **128** (2005), 240–250. https://doi.org/10.1115/1.2150834
34. K. Zaimi, A. Ishak, I. Pop, Unsteady flow due to a contracting cylinder in a nanofluid using Buongiorno's model, *Int. J. Heat Mass Transfer*, **68** (2014), 509–513. https://doi.org/10.1016/j.ijheatmasstransfer.2013.09.047
35. A. Hussain, M. Y. Malik, T. Salahuddin, S. Bilal, M. Awais, Combined effects of viscous dissipation and Joule heating on MHD Sisko nanofluid over a stretching cylinder, *J. Mol. Liq.*, **231** (2017), 341–352. https://doi.org/10.1016/j.molliq.2017.02.030
36. L. Ali, X. Liu, B. Ali, S. Mujeed, S. Abdal, Finite element simulation of multi-slip effects on unsteady MHD bioconvective micropolar nanofluid flow over a sheet with solutal and thermal convective boundary conditions, *Coatings*, **9** (2019), 842. https://doi.org/10.3390/coatings9120842
37. N. Abbas, S. Nadeem, A. Saleem, M. Y. Malik, A. Issakhov, F. M. Alharbi, Models base study of inclined MHD of hybrid nanofluid flow over nonlinear stretching cylinder, *Chin. J. Phys.*, **69** (2021), 109–117. https://doi.org/10.1016/j.cjph.2020.11.019
38. A. E. Shafey, F. M. Alharbi, A. Javed, N. Abbas, H. A. ALrafai, S. Nadeem, et al., Theoretical analysis of Brownian and thermophoresis motion effects for Newtonian fluid flow over nonlinear stretching cylinder, *Case Stud. Therm. Eng.*, **28** (2021), 101369. https://doi.org/10.1016/j.csite.2021.101369
39. N. Abbas, K. Ur Rehman, W. Shatanawi, A. A. Al-Eid, Theoretical study of non-Newtonian micropolar nanofluid flow over an exponentially stretching surface with free stream velocity, *Adv. Mech. Eng.*, **14** (2022). https://doi.org/10.1177/16878132221107790
40. N. Abbas, K. Ur Rehman, W. Shatanawi, K. Abodayeh, Mathematical model of temperature-dependent flow of power-law nanofluid over a variable stretching Riga sheet, *Waves Random Complex Media*, 2022. https://doi.org/10.1080/17455030.2022.2111029

41. L. Ali, B. Ali, M. B. Ghori, Melting effect on Cattaneo-Christov and thermal radiation features for aligned MHD nanofluid flow comprising microorganisms to leading edge: FEM approach, *Comput. Math. Appl.*, **109** (2022), 260–269. https://doi.org/10.1016/j.camwa.2022.01.009
42. L. Ali, Y. J. Wu, B. Ali, S. Abdal, S. Hussain, The crucial features of aggregation in TiO_2-water nanofluid aligned of chemically comprising microorganisms: a FEM approach, *Comput. Math. Appl.*, **123** (2022), 241–251. https://doi.org/10.1016/j.camwa.2022.08.028
43. P. Kumar, H. Poonia, L. Ali, S. Areekara, The numerical simulation of nanoparticle size and thermal radiation with the magnetic field effect based on tangent hyperbolic nanofluid flow, *Case Stud. Therm. Eng.*, **37** (2022), 102247. https://doi.org/10.1016/j.csite.2022.102247
44. M. Qasim, Z. H. Khan, W. A. Khan, I. Ali Shah, MHD boundary layer slip flow and heat transfer of ferrofluid along a stretching cylinder with prescribed heat flux, *Plos One*, **9** (2014), e83930. https://doi.org/10.1371/journal.pone.0083930
45. M. Suleman, M. Ramzan, S. Ahmad, D. Lu, Numerical simulation for homogeneous-heterogeneous reactions and Newtonian heating in the silver-water nanofluid flow past a nonlinear stretched cylinder, *Phys. Scr.*, **94** (2019), 085702. https://doi.org/10.1088/1402-4896/ab03a8

AIMS Press